Dalton Transactions

PAPER

View Article Online
View Journal | View Issue

Cite this: *Dalton Trans.*, 2015, **44**, 4088

The catalytic performance of metal complexes immobilized on SBA-15 in the ring opening polymerization of ε-caprolactone with different metals (Ti, Al, Zn and Mg) and immobilization procedures†

Yolanda Pérez,*[a] Isabel del Hierro,*[a] Lydia Zazo,[a] Rafael Fernández-Galán[b] and Mariano Fajardo[a]

Received 4th November 2014,
Accepted 8th January 2015

DOI: 10.1039/c4dt03385j

www.rsc.org/dalton

A family of heterogeneous catalysts has been prepared by employing different strategies: firstly by direct reaction or grafting of titanium, zinc, aluminium and magnesium precursors with dehydrated SBA-15 and secondly by reaction of the metallic derivatives with a hybrid SBA-15 mesoporous material, which possesses a new covalently bonded linker based on an amino alcohol chelate ligand. These materials have been characterized by X-ray diffraction (XRD), X-ray fluorescence (XRF), N_2 adsorption–desorption, FT-IR and multi-nuclear NMR spectroscopy. The catalytic performance of the prepared materials has been studied in the ring opening polymerization of ε-caprolactone and compared with that of their homogeneous counterparts. Conversion values obtained by using homogeneous and heterogeneous catalysts depend on the metal precursor and the synthetic procedure. The most active heterogeneous Ti-SBA-15, Zn-SBA-15 and Zn-PADO-HMDS-SBA-15 catalysts produced poly(ε-caprolactone) with a narrow molecular weight distribution, close to one. In all cases polymerization was confirmed to proceed *via* a coordination insertion mechanism after end group analysis by ^{1}H NMR.

Introduction

Conventional plastics possess excellent properties. However, the high durability of these synthetic polymers has caused a crisis in solid waste management. New regulations affecting packaging producers will force them to take charge of their waste in the future.[1] In response, industries and the scientific community have enhanced research into new materials compatible with the environment. Biodegradable polymers, poly (caprolactone) (PCL), polyglycolide (PGA), polylactide (PLA) and their copolymers, besides their bulk applications in packaging and various other consumer goods, are particularly interesting for medicine and tissue engineering purposes due to their biocompatibility. Particularly, interest toward polycaprolactone (PCL) homopolymers for medical devices has extensively increased ever since it was discovered that it is a suitable scaffold material for cells in repairing and regenerating tissue defects and can act as a drug delivery agent.[2,3] The biodegradability of poly(ε-caprolactone)[4] and its copolymers with available renewable resources (lactide or glycolide)[5,6] has made it a preferred choice for potential environmentally friendly commodity plastics and the demand for this polymer is ever increasing.

An upcoming challenge is to produce biodegradable polymers or copolymers based on poly(ε-caprolactone) at low cost and with physical properties that would make them industrial competitors to non-biodegradable, well established commodity polymers such as poly(ethylene). These polyesters are most commonly produced by ring opening polymerizations (ROPs) of the cyclic esters using cationic, anionic and coordination–insertion polymerization techniques.[7] The latter has received significant attention as it offers an efficient method to control the molecular weight and molecular weight distribution of the polyesters and thus, these properties of polyesters can be modified with great precision.

Homogeneous catalysts have been designed that can control polymer molecular weights, molecular weight distri-

[a]*Departamento Biología y Geología, Física y Química Inorgánica (E.S.C.E.T.), Universidad Rey Juan Carlos, 28933 Móstoles, Madrid, Spain. E-mail: yolanda.cortes@urjc.es, isabel.hierro@urjc.es; Fax: (+34) 914888143; Tel: (+34) 914887022*

[b]*Departamento Química Inorgánica, Orgánica y Bioquímica, Facultad de Ciencias y Tecnologías Químicas, Universidad de Castilla-La Mancha, Campus Universitario de Ciudad Real, 13071-Ciudad Real, Spain*

†Electronic supplementary information (ESI) available. See DOI: 10.1039/c4dt03385j

butions, co-monomer incorporation and stereochemistry. Typical single site catalysts for lactone polymerization are of the form $M(OR)L_n$, where the alkoxy group (OR) is capable of propagation. These complexes are conceptually different from typical lactone polymerization catalysts of the form $M(OR)_n$, which do not possess a permanent ancillary ligand.[8] A large variety of new single site catalytic systems based on tin,[9] aluminium,[10,11] zinc,[12] magnesium,[13] iron,[14] lanthanide,[15] titanium[16] and lithium[17] organometallic complexes containing initiating groups such as amides, carboxylates, and alkoxides have been reported.[18,19]

From a practical point of view, it would be desirable for these catalysts to be heterogeneous to allow for better control of the polymerization process and easier separation of the catalysts from the polymer product and some examples have been reported in recent years of immobilization of metallic precursors on inorganic supports. Homoleptic alkoxy complexes, such as titanium and calcium alkoxy complexes, have been supported on silica substrates by Chung[20] and George,[21] respectively, to prepare catalysts active in the polymerization of L-lactide and ε-caprolactone (ε-CL). Previously, Jérôme prepared silica supported [tris(hexamethyldisilyl)amide]yttrium to use this material as an initiator in the ROP of ε-CL in the presence of 2-propanol[22] and Spitz *et al.* have published the synthesis of silica grafted lanthanide amide and its transformation into an alkoxide, and tested this new material in the ROP of ε-CL in the presence of benzyl alcohol.[23]

Single site catalysts are also useful precursors. C. W. Jones *et al.* have anchored β-diiminate zinc alkoxy complexes onto SBA-15 for polymerization of lactides.[24] Recently, M. D. Jones and co-workers have published the tethering of zinc[25] and aluminium Schiff bases onto silica and their behaviour as catalysts in the polymerization of *rac*-lactide.[26]

A different approach has been used to prepare alternative supports. C. W. Jones *et al.* have published the preparation of magnetic nanoparticle supported aluminium isopropoxy as a new catalyst for the ring-opening polymerization of ε-CL.[27] Tantirungrotechai and co-workers have successfully used aluminium and calcium-incorporated MCM-41-type silica as catalytic supports for the polymerization of L-lactide and ε-CL, the catalytic centres were generated by grafting titanium(IV) isopropoxide onto the support.[28]

Among the inert supports used in the last decade, for the heterogenization of catalytically active species, well ordered mesoporous silica is without doubt one of the most promising materials. The support used in the present study SBA-15 has become the most popular member of the highly ordered mesoporous (20–300 Å) silica structure family synthesized by the use of commercially available poly(alkylene oxide) triblock copolymer surfactant species. SBA-15 has a two-dimensional *p6mm* hexagonal structure, with a well ordered hexagonal array and one-dimensional channel structure. It possesses high thermal stability, very high surface area (>800 $m^2\ g^{-1}$), and pores large enough (8 to 11 nm) to immobilize molecular catalysts (*e.g.* metal complexes), and its uniformly sized and shaped tunable pores have the potential to induce shape selectivity in the local environment of the active centre. Another important aspect of SBA-15 materials is linked to the commercial requirements for their synthesis. There is a strong demand for low cost processes, scaling up the batch size, high yields and synthesis efficiency.[29]

In this study, new mesoporous heterogeneous catalysts have been prepared by different strategies. The post-grafting process through covalent linkage of surface silanol groups and active titanium, aluminium, magnesium and zinc precursors has been regarded as an alternative route for the preparation of metal ion doped mesoporous materials. This process avoids the introduction of heteroatoms into the framework of the ordered mesostructures and the catalytically active centres are located at the pore surface, which are easily accessible to the reactants. However, the formation of oligomeric species causes the immobilization of active groups onto the support through coordination of the metal to a terminal functional group of a surface bound linker, based on an amino alcohol chelate ligand, a good alternative that ensures the purity of the pseudo-homogeneous complex present on the support. The catalytic performance of the prepared materials has been studied in the ring opening polymerization of ε-CL and compared with that of their homogeneous counterparts.

Experimental section

General procedures

All reactions were performed using standard Schlenk tube techniques under an atmosphere of dry nitrogen or argon. Tetraethylorthosilicate (TEOS) 98% (M = 208.33, d = 0.934 g mL^{-1}), poly(ethylene glycol)-*block*-poly(propylene glycol)-*block*-poly(ethylene glycol) (M_{av} = 5800, d = 1.007 g mL^{-1}), hexamethyldisilazane (HMDS) (M = 161.39, d = 0.774 g mL^{-1}), dimethyl zinc ($ZnMe_2$) 2 M in toluene, 3-[bis(2-hydroxyethyl) amino]propyl-triethoxysilane solution 65% in ethanol (M = 309.47, d = 0.94 g mL^{-1}), di-*n*-butylmagnesium ($Mg(^nBu)_2$) 1 M in heptane (M = 138.53, d = 0.713 g mL^{-1}), methyl aluminium ($AlMe_3$) 2 M in toluene (M = 72.09, d = 0.752 g mL^{-1}) and aluminium isopropoxide ($Al(O^iPr)_3$) (M = 204.24) were purchased from Sigma Aldrich and used as received. Titanium tetraisopropoxide 97% ($Ti(O^iPr)_4$) (M = 284.22, d = 0.955 g mL^{-1}) was purchased from Sigma Aldrich and was distilled and stored under a nitrogen atmosphere prior to use. ε-Caprolactone (M = 114.14, d = 1.003 g mL^{-1}) was purchased from Fluka, and was refluxed over CaH_2, distilled and stored under a nitrogen atmosphere prior to use. Hydrochloric acid 35% was purchased from Panreac. Organic solvents were purchased from SDS and were distilled and dried before use according to conventional literature methods. Water was obtained using a Millipore Milli-Q system (Waters, USA). The hexagonal material (SBA-15) was prepared using a poly(alkaline oxide) triblock copolymer surfactant in an acidic medium, according to the method of Zhao *et al.*[29a] Silica was purchased from Sigma Aldrich. Homogeneous titanium and zinc catalysts designated

as Ti-PADO and Zn-PADO have been synthesized according to previously published procedures.[30]

Characterization

X-ray diffraction (XRD) patterns of the silicas were obtained on a Phillips Diffractometer model PW3040/00 X'Pert MPD/MRD at 45 kV and 40 mA, using Cu-Kα radiation (λ = 1.5418 Å). N_2 gas adsorption–desorption isotherms were obtained using a Micromeritics TriStar 3000 analyzer, and pore size distributions were calculated using the Barret–Joyner–Halenda (BJH) model on the adsorption branch. Infrared spectra were recorded on a Nicolet-550 FT-IR spectrophotometer (in the region 4000 to 400 cm^{-1}) as Nujol mulls between polyethylene pellets and KBr disks. Proton-decoupled ^{29}Si MAS NMR spectra were recorded on a Varian-Infinity Plus 400 MHz spectrometer operating at 79.44 MHz proton frequency (4 μs 90° pulse, 1024 transients, spinning speed of 5 MHz). Cross-polarization ^{13}C CP/MAS NMR spectra were recorded on a Varian-Infinity Plus 400 MHz spectrometer operating at 100.52 MHz proton frequency (4 μs 90° pulse, 4000 transients, spinning speed of 6 MHz, contact time 3 ms, pulse delay 1.5 s). Elemental analysis (% C and % N) was performed by the Investigation Service of Universidad de Alcalá (Spain) using a CHNS analyser LECO-932 model. The titanium, aluminium, magnesium and zinc contents were determined from XRF scanning electron micrographs and morphological analysis was carried out on a XL30 ESEM Philips. The DR UV-Vis spectroscopic measurements were carried out on a Varian Cary-500 spectrophotometer equipped with an integrating sphere and polytetrafluoroethylene (PTFE) was used as the reference, with d = 1 g cm^{-3} and the thickness of 6 mm. The electronic absorption UV-vis spectra were recorded in a toluene solution on a UV-Vis Analytik Jena Specord 200PC spectrophotometer. Thermogravimetric analysis was performed using a Setsys 18 A (Setaram) thermogravimetric analyzer.

Synthesis

Synthesis of homogeneous Al and Mg complexes. An equimolar amount of $AlMe_3$, 2 M in toluene (1.00 mL, 2.0 mmol) was added to a toluene solution (25 mL) of 3-[bis(2-hydroxyethyl)amino]propyl-triethoxysilane (65%) in ethanol (1.06 mL, 2.0 mmol) at 0 °C. The reaction evolves with methane elimination as the temperature increases to room temperature. The solution was stirred for 4 h, afterwards the solvent was removed *in vacuo*, and the resulting solid was washed with hexane (2 × 10 mL) to give the complex Al(Me)-PADO as a white solid. In a similar way complexes Al-PADO and Mg-PADO have been prepared by using equimolar amounts of $Al(O^iPr)_3$ (0.2 g, 2.0 mmol) and $Mg(^nBu)_2$ (1.00 mL, 2 mmol) toluene solutions to obtain white solids sparingly soluble in toluene.

Synthesis of heterogeneous catalysts

Grafting of $Ti(O^iPr)_4$, $ZnMe_2$, $Mg(^nBu)_2$ or $Al(O^iPr)_3$ onto SBA-15. 1 g of SBA-15 previously dehydrated at 150 °C over 15 h was suspended in 50 mL of dry toluene, and to the mechanically stirred suspension $Ti(O^iPr)_4$ (1.2 mL, 4 mmol), $ZnMe_2$ (2.0 mL, 4 mmol) or $Mg(^nBu)_2$ (4.8 mL, 4 mmol) was added using a syringe. $Al(O^iPr)_3$ (0.8 g, 4 mmol) was previously dissolved in 10 mL of dry toluene and transferred to the SBA-15 suspension. In all cases the reactant mixture was stirred at room temperature for 24 h. The solid was filtered off, washed repeatedly with toluene and hexane, dried under vacuum and stored under an inert atmosphere. The obtained materials have been labelled as Ti-SBA-15, Zn-SBA-15, Mg-SBA-15 and Al-SBA-15, respectively.

Functionalization of SBA-15 with 3-[bis(2-hydroxyethyl)amino]-propyl-triethoxysilane in the presence of hexamethyldisilazane as the capping agent. In a typical experiment 1 g of SBA-15 silica was suspended in 30 mL of dry toluene, and hexamethyldisilazane (HMDS) (0.84 mL, 4 mmol) and 3-[bis(2-hydroxyethyl)-amino]propyl-triethoxysilane in an ethanol solution (2 mL, 4 mmol) were added in turns. The reaction mixture was stirred for 24 h at 90 °C and the resulting solid labelled with the acronym of PADOH-HMDS-SBA-15, was filtered off and washed with toluene (2 × 50 mL) and hexane (1 × 50 mL). The final material was dried under vacuum and stored under an inert atmosphere.

Tethering of $Ti(O^iPr)_4$, $ZnMe_2$, $AlMe_3$, $Al(O^iPr)_3$ or $Mg(^nBu)_2$ onto PADO-HMDS-SBA-15. 1 g of PADO-HMDS-SBA-15 was dissolved in dry toluene (45 mL) and reacted with an excess of $Ti(O^iPr)_4$, $ZnMe_2$, $AlMe_3$, $Al(O^iPr)_3$ or $Mg(^nBu)_2$, (4 mmol), respectively. The reaction mixture was stirred at room temperature for 24 h and the final product was collected by filtration and washed with dry toluene (2 × 50 mL) and with hexane (1 × 50 mL). The obtained materials, designated as Ti-PADO-HMDS-SBA-15, Zn-PADO-HMDS-SBA-15, Al(Me)-PADO-HMDS-SBA-15, Al-PADO-HMDS-SBA-15 and Mg-PADO-HMDS-SBA-15, were dried under vacuum and stored under an inert atmosphere.

ε-Caprolactone polymerization

Polymerization of ε-caprolactone was carried out under an inert atmosphere using a flask equipped with a magnetic stirrer. Predetermined amounts of purified ε-CL, dried toluene, and the homogeneous or heterogeneous catalyst were charged and the monomer was added using a syringe with vigorous magnetic stirring. The polymerization studies were carried out at room temperature and 80 °C, for homogeneous catalysts and heterogeneous catalysts, respectively. In kinetic or mechanism studies in the homogeneous phase small aliquots were taken at different reaction times depending on the catalyst (see the Results and discussion section). After the reaction time had elapsed the ε-CL polymerization was quenched by addition of 5 mL of methanol, the solid phase was separated by filtration and the polymer was precipitated with an excess of methanol. The polymer was washed with methanol and dried at 50 °C under vacuum for 12 h. The sample was subjected to ^1H NMR spectroscopy ($CDCl_3$) and gel permeation chromatography (GPC) to determine the average molecular weights M_n, M_w of the produced polymer and molecular weight distribution (PDI). The monomer conversion was determined from the relative intensity of the NMR signals at δ 4.20

and 4.02 ppm corresponding to the OCH_2 resonance in ε-caprolactone and poly(ε-caprolactone), respectively.

Results and discussion

Synthesis of titanium, zinc, aluminium and magnesium mesoporous M-SBA-15 and analogous metallic hybrid M-PADO-HMDS-SBA-15 materials

The materials Ti-SBA-15, Zn-SBA-15, Al-SBA-15 and Mg-SBA-15 have been prepared by direct reaction of 1 g of SBA-15 mesoporous silica, previously dehydrated, with 4 mmol of $Ti(O^iPr)_4$, $ZnMe_2$, $Al(O^iPr)_3$ or $Mg(^nBu)_2$ in toluene under an inert atmosphere for 24 h (Scheme 1). This process avoids the introduction of heteroatoms into the framework of the ordered mesostructure and guarantees that the chemically active metallic centres are located at the pore surfaces of the parent SBA-15.

Alternatively, an organic–inorganic hybrid SBA-15 material has been synthesized slightly modifying published procedures.[31,32] The material with the acronym PADOH-HMDS-SBA-15 has been prepared by one step reaction of dehydrated SBA-15 with a mixture of silylating agents, an alkoxysilane compound, 3-[bis(2-hydroxyethyl)amino]propyltriethoxysilane (PADOH) and the silylamine, hexamethyldisilazane (HMDS), a capping agent capable of masking the remaining silanol groups available on the silica surface and of increasing the surface hydrophobicity. In the second stage titanium, zinc, aluminium and magnesium materials have been obtained by tethering the corresponding alkoxy or alkyl metallic precursor onto organomodified or PADOH-HMDS-SBA-15 (Scheme 2). The immobilization of active groups onto the silica support through coordination of a metal to a covalently bonded linker based on an amino alcohol chelate ligand should ensure the purity of pseudo-homogeneous single site complexes present on the support.

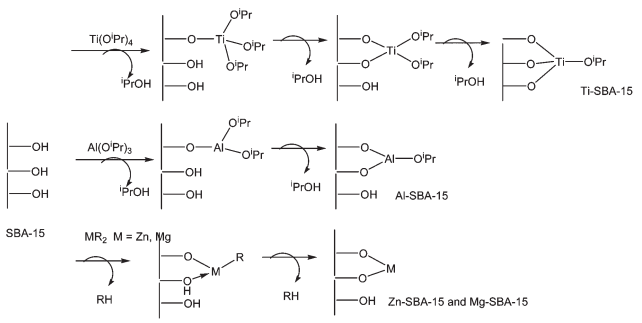

Scheme 1 Preparation of Ti-SBA-15, Zn-SBA-15, Al-SBA-15 and Mg-SBA-15 materials.

Characterization of titanium, zinc, aluminium and magnesium mesoporous SBA-15 and hybrid PADO-HMDS-SBA-15 materials

XRD patterns of the organic–inorganic hybrid material are similar to those of the corresponding parent support, revealing the (100) reflection peak at $2\theta \cong 0.92$ characteristic of the hexagonally ordered arrangement of SBA-15 (Fig. 1). The *d*-spacing value for this XRD peak is 96.02 Å and a_0 is equal to 110.88 Å. The results confirm that the ordered mesoporous structure of SBA-15 remains intact after the functionalization procedure with PADOH or the mixture PADOH/HMDS. An overall decrease in intensity is observed which can be attributed to the lowering local order, such as variations in the wall thickness of the framework or reduction of scattering contrast between the channel wall and the ligands present on the inner surface of SBA-15 (Table 1). As an example, similar behaviour is observed by studying the diffractograms of Al-PADO-HMDS-SBA-15; compared to parent SBA-15 the aluminium tethered sample shows an important decrease in the relative intensities of the XRD.

The N_2 adsorption–desorption isotherms of hybrid materials can be classified as type IV characteristic of mesoporous materials (Fig. 2, S1 and S2†). The mesopores are uniform in size, which is indicated by the sharp increase in N_2 uptake for adsorption, observed at P/P_0 *ca.* 0.50–0.70. After silylation and aminediol ligand incorporation a drastic decrease in the S_{BET}, pore volume and average BJH pore diameter was observed (see Table 1), changes that can be interpreted as being due to the presence of organic molecules anchored to the channels partially blocking the adsorption of nitrogen molecules. Since most of the aminediol sites which can bind with active metal centres in PADOH-HMDS-SBA-15 are located at the surface, it is clearly seen that the surface area and pore volume gradually decrease with subsequent complexation with metal ions. Thus, we can conclude that the organic moiety as well as the metal ions are grafted inside the mesopore cavity.

The nitrogen content obtained by elemental analysis for PADOH-SBA-15 and PADOH-HMDS-SBA-15 was 1.44% and

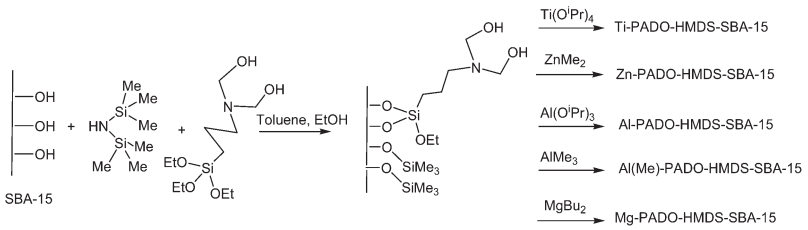

Scheme 2 Preparation of Ti-PADO-HMDS-SBA-15, Zn-PADO-HMDS-SBA-15, Al-PADO-HMDS-SBA-15, Al(Me)-PADO-HMDS-SBA-15 and Mg-PADO-HMDS-SBA-15 materials.

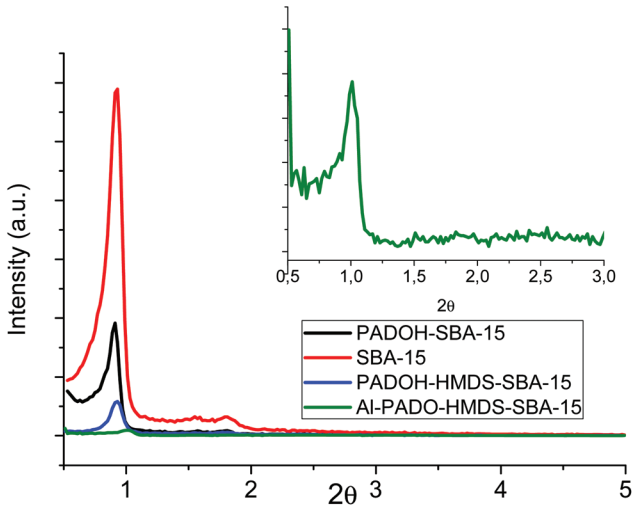

Fig. 1 XRD patterns of SBA-15; PADOH-SBA-15, PADOH-HMDS-SBA-15 and Al-PADO-HMDS-SBA-15.

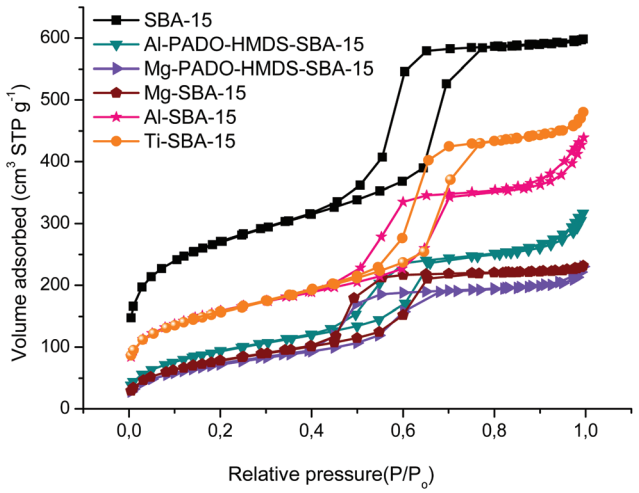

Fig. 2 Nitrogen adsorption–desorption isotherm profiles of Mg-SBA-15; Al-SBA-15, Mg-PADO-HMDS-SBA-15 and Al-PADO-HMDS-SBA-15.

0.94%, respectively (Table 2). The aminediol based ligand loading was found to be 1.03 and 0.67 mmol g^{-1}. Taking into account these values and S_{BET} of the parent mesoporous silica, the average surface density (d, molecules nm^{-2}) of the attached molecules and the average intermolecular distance (l, nm) were calculated. The values obtained were d = 0.70 and l = 1.20 nm for PADOH-SBA-15 and d = 0.46 and l = 1.48 nm for PADOH-HMDS-SBA-15. On the basis of carbon and nitrogen content measurements the amount of the capping ligand was also calculated for PADOH-HMDS-SBA-15 using the following expression: mmol capping agent g^{-1} = mmolC g^{-1} (mmolN g^{-1} × nC), where nC = the number of carbon atoms in PADOH and assuming total condensation, three surface silanol groups react with three ethoxy groups (–OC_2H_5). The obtained value 8.04 mmol HMDS g^{-1} suggests that under the prevailing experimental conditions the competitive silylation reaction achieved a higher –$SiMe_3$ surface coverage.

The metal loading was calculated by X-ray fluorescence (XRF) analysis. Considering that the hybrid organic–inorganic materials, metal complexes, are anchored *via* the incorporated ligand into the mesoporous silica, the anchoring efficiency of the metal toward the linker can be estimated taking into account the amount of the incorporated ligand and metal loading. The measured metal content for Ti and Zn-PADO-HMDS-SBA-15 is 4.14 and 2.04%, respectively, which corresponds to 0.86 and 0.84 mmol g^{-1}. These data show a molar ratio or metal : ligand ratio close to one which suggests the formation of titanium and magnesium complexes with 1 : 1 stoichiometry. The ratio of metal to ligand obtained for zinc hybrid mesoporous materials increases significantly, supporting a better anchoring efficiency and the formation of complexes with 1 : 2 stoichiometry. In the case of aluminium the immobilization efficiency is slightly higher for $AlMe_3$ in comparison with $Al(O^iPr)_3$, yielding anchored complexes with 1 : 1 stoichiometry (see Table 1).

The hybrid materials were also characterized by ^{29}Si and ^{13}C MAS NMR. As an example, ^{29}Si MAS NMR spectra of PADOH-HMDS-SBA-15 and Al-PADO-HMDS-SBA-15 are shown in Fig. 3. The spectra of the functionalized silica show two main peaks at −110 and −101 ppm assigned to Q^4 framework

Table 1 Textural properties and metal content of the mesoporous SBA-15 materials

Material	S_{BET} (m^2 g^{-1})	Pore volume (cm^3 g^{-1})	Pore size (Å)	Metal content[a] (%)	Metal content[a] (mmol g^{-1})
SBA-15	886	1.03	57	—	
PADOH-SBA-15	463	0.56	55	—	
PADOH-HMDS-SBA-15	390	0.50	54	—	
Ti-SBA-15	557	0.70	51	15.50	3.24
Zn-SBA-15	626	0.95	55	12.80	1.96
Al-SBA-15	610	0.81	53	6.89	2.55
Mg-SBA-15	292	0.35	48	4.85	2.00
Zn-PADO-HMDS-SBA-15	311	0.40	51	9.42	1.44
Al-PADO-HMDS-SBA-15	352	0.44	52	2.56	0.95
Al(Me)-PADO-HMDS-SBA-15	292	0.44	53	2.91	1.08
Mg-PADO-HMDS-SBA-15	270	0.32	48	2.04	0.84
Zn-PADO-HMDS-Silica	194	0.32	65	12.50	1.91

[a] The metal content was calculated by X-ray fluorescence (XRF) analysis.

Table 2 C and N contents (wt%) obtained by elemental chemical analysis (CNH)

Material	%N	%C	mmol N (g^{-1})	mmolC (g^{-1})	mmol Ligand[a] (g^{-1})	mmol capping agent[b] (g^{-1})	Surface coverage[c] (the number of PADOH/ PTDOH per nm^2)	Capping agent/ ligand ratio
PADOH-SBA-15	1.44	14.55	1.03	12.13	1.03		0.70	
PADOH-HMDS-SBA-15	0.94	13.68	0.67	11.40	0.67	8.04	0.46	11.98

[a] mmol ligand g^{-1}, calculated from mmol N g^{-1} values since the PADOH ligand possesses one nitrogen atom in its structure. [b] mmol capping agent (hexamethyldisilazane) g^{-1}, calculated from C mmol g^{-1} values. mmol capping agent g^{-1} = C mmol g^{-1} (N mmol g^{-1} × nC), where nC = the number of carbon atoms in the PADOH ligand assuming total condensation, three surface silanol groups react with three ethoxy groups ($-OC_2H_5$). [c] Surface coverage: example: α(PADOH) = δ(PADOH)$N_A a_s^{-1}$ × 10^{-18} (the number of PADOH groups per nm^2), δ(PADOH) = %N$(100 n_N M_N)^{-1}$ [mol g^{-1}] = the concentration of surface PADOH groups, %N = wt% refers to the parent SBA-15 silica; N_A = the Avogadro constant (6.022×10^{23} mol^{-1}); a_s = the specific BET surface area of the dehydrated, non-modified SBA-15 (886 m^2 g^{-1}); n_N = the number of nitrogen atoms per PADOH group (–N–((CH_2)–OH)$_2$, 1); M_C = the atomic weight of nitrogen (14.010 g mol^{-1}).

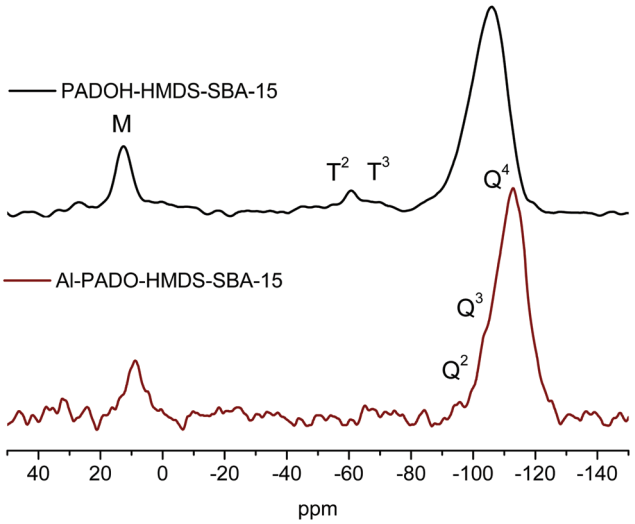

Fig. 3 ^{29}Si MAS NMR spectrum of PADOH-HMDS-SBA-15 and Al-PADO-HMDS-SBA-15.

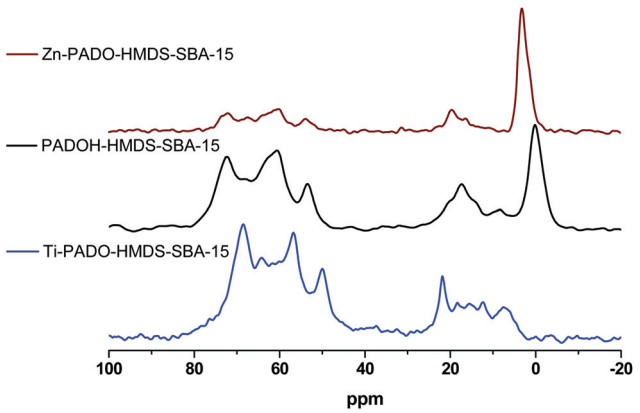

Fig. 4 ^{13}C MAS NMR spectra of Zn-PADO-HMDS-SBA-15, PADOH-HMDS-SBA-15 and Ti-PADO-HMDS-SBA-15 materials.

silica sites ($(SiO)_4Si$) and Q^3 silanol sites ($(SiO)_3SiOH$), respectively. A marked decrease in the intensity of the Q^3 signal in comparison with parent SBA-15 is observed, which verified the tethering of the functional groups to Si–OH. T^2 ($RSi(OSi)_2(OR')$) and T^3 ($RSi(OSi)_3$) organosilane species at −57 and −63 ppm, respectively, present in the functionalized material are indicative of a high degree of condensation of the triethoxysilanes with the silica surface. In addition, the choice of HMDS as the protecting group allows easy determination of the trimethylsilyl groups by ^{29}Si NMR; the new peak of the silylating agent, an M site ($(Me_3SiO–$), is seen at 12 ppm.

^{13}C CP MAS NMR studies provide useful information regarding the presence of an organic moiety and the chemical interaction of metal ions with the donor sites in the hybrid frameworks. In Fig. 4 the ^{13}C CP MAS NMR spectra of metal containing materials are shown in comparison with the parent PADOH-HMDS-SBA-15. The spectrum for the metal free aminediol ligand containing mesoporous material exhibits three signals from the three carbon atoms present in the alkyl chain at 7, 16 and 58 ppm for ≡Si–CH_2–, CH_2–CH_2–CH_2– and –CH_2–O, respectively. In addition two additional signals at 16 and 50 ppm attributed to the unreacted ethoxy groups attached to Si in the aminediol silane ligand are observed. The signal attributed to methylenic carbons –N–(CH_2–OH)$_2$ of the aminediol ligand appears at 69 ppm. As characteristic signals in Ti-PADO-HMDS-SBA-15 it is worth mentioning the signals of the isopropoxy ligand at 21 and 64 ppm for methyl (CH_3)$_2$–CH–O and methyne (CH_3)$_2$–CH–O groups, respectively. The spectrum of Zn-PADO-HMDS-SBA-15 shows an identical pattern to that of the parent material.

In order to obtain extra information about the possible structure of the catalyst, two aluminium precursors have been anchored on the aminediol based SBA-15 material. Fig. 5 shows the ^{13}C CP MAS NMR spectra of both materials that confirm the presence of different aluminium complexes immobilized on the silica surface depending on the metal precursor. As significant signals the spectrum of the material synthesized by using $AlMe_3$ shows a sharp signal at 2 ppm attributed to the methyl group directly bonded to aluminium, meanwhile the spectrum of the material synthesized by using $Al(O^iPr)_3$ shows at 21 ppm the characteristic signal of the methyl groups (CH_3)$_2$–CH–O in the isopropoxy ligand. ^{27}Al solid state NMR spectroscopy is a good tool for the determination of the aluminium coordination number in complexes. It is well known that ^{27}Al solid state NMR spectra show a

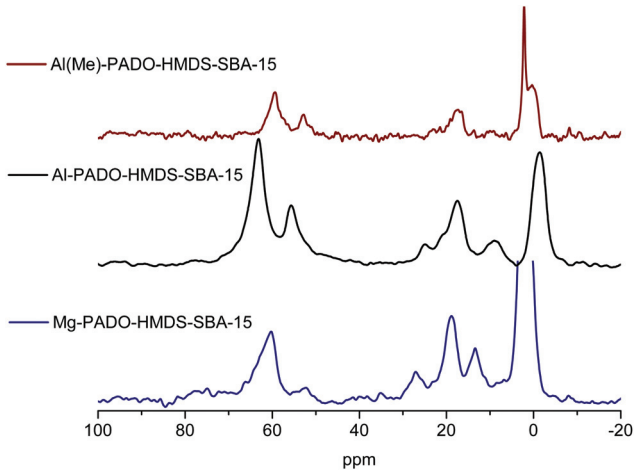

Fig. 5 ^{13}C CP MAS NMR spectra of Al(Me)-PADO-HMDS-SBA-15, Al-PADO-HMDS-SBA-15 and Mg PADO-HMDS-SBA-15 materials.

signal between −10 and +20 ppm for the coordination number six and between +55 and +85 ppm for the coordination number four. Some rare examples of five-coordinate aluminium are known, with signals near +35 ppm. Fig. 6 shows the ^{27}Al NMR CP NMR spectra of Al(Me)-PADO-HMDS-SBA-15 and Al-PADO-HMDS-SBA-15; two signals at 58 and 5 ppm are observed for the first material, which clearly indicates the

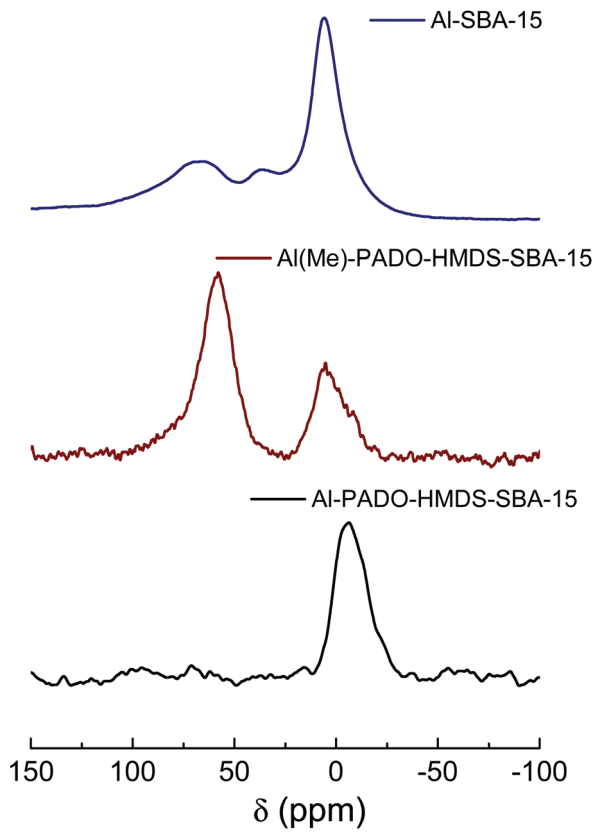

Fig. 6 ^{27}Al CP MAS NMR spectra of Al-SBA-15, Al(Me)-PADO-HMDS-SBA-15 and Al-PADO-HMDS-SBA-15.

presence of aluminium centres with different coordination environments, four and six, respectively when the metallic precursor employed in the immobilization procedure is $AlMe_3$. If $Al(O^iPr)_3$ is used instead, the aluminium atoms are probably octahedrally coordinated as made evident by the presence of only one signal at – 6 ppm.[33] Finally, in the ^{27}Al NMR spectrum of Al-SBA-15 three resonances are observed at 6, 37 and 66 ppm, for tetrahedral, 5 coordinate and octahedral aluminium environments. Taking into account the experimental results, the proposed structures for the materials synthesized using two different aluminium precursors are shown in Fig. 7a and b.

FT-IR spectra of the mesoporous SBA-15 silica heterogenized aminediol ligand with and without the presence of capped trimethylsilyl groups have been recorded before and after metal immobilization, as well as FT-IR spectra of parent SBA-15 before and after metal immobilization between 4000 and 400 cm^{-1} (Fig. 8 and 9). The main features of the SBA-15 spectra include a large broad band between 3400 and 3200 cm^{-1}, which is attributed to O–H stretching of the surface silanol groups and the remaining adsorbed water molecules. The siloxane (–Si–O–Si–) band appears as a broad strong peak centred at 1100 cm^{-1}. The band due to Si–O bond stretching of the silanol groups was observed at 960 cm^{-1}. The adsorption band at 1630 cm^{-1} is due to deformation vibrations of the adsorbed water molecules.[34] After functionalization with 3-[bis(2-hydroxyethyl)amino]propyl-triethoxysilane the absorption peaks of the Si–OH groups and physisorbed water decrease, new bands appear in the range 2873–2964 attributed to the ν(C–H) stretching vibrations, at 1459 and 1353 cm^{-1} and in the range 764–843 cm^{-1} assigned to the $\gamma(-CH_2-)$ alkyl chain due to the anchored ligand (Fig. S3†). After the one pot reaction with an equimolar mixture of 3-[bis(2-hydroxyethyl)-amino]propyl-triethoxysilane and hexamethyldisilazane a similar pattern is observed with the addition of HMDS with a strong band at 798 cm^{-1} $\gamma(-CH_3)$ belonging to the $Me_3Si–O–Si\equiv$ groups on the silica surface (Fig. S3†). Fig. 8 and S4† show some of the above mentioned spectra and those obtained upon metal immobilization. As can be seen the formation of the anchored complexes on the silica surface does not modify the FT-IR spectra significantly.

Fig. 9 shows the spectra of those materials prepared by direct immobilization of $Ti(O^iPr)_4$, $ZnMe_2$, $Al(O^iPr)_3$ or $Mg(^nBu)_2$ on the previously dehydrated silica surface. All spectra have in common the presence of ν(C–H) stretching vibrations in the range 2858–2962 cm^{-1} which supports the presence of ligands, alkoxy or alkyl chains, directly bonded to the metal atoms. For Ti-SBA-15 and Al-SBA-15 the bands typical of isopropoxy groups bonded to metal anchored complexes appear at 1466 cm^{-1} ($\delta_a(CH_2)$, $\delta_a(CH_3)$) and 1385 cm^{-1} $\delta_s(CH_3)$; meanwhile the presence of a band at 950 cm^{-1} is clear evidence of the presence of Ti anchored onto the silica surface, since this absorption is due to the antisymmetric Ti–O–Si stretching vibration. As previously reported, grafting reactions of isopropoxy titanium and aluminium complexes may occur with different possible stoichiometries through tripodal,

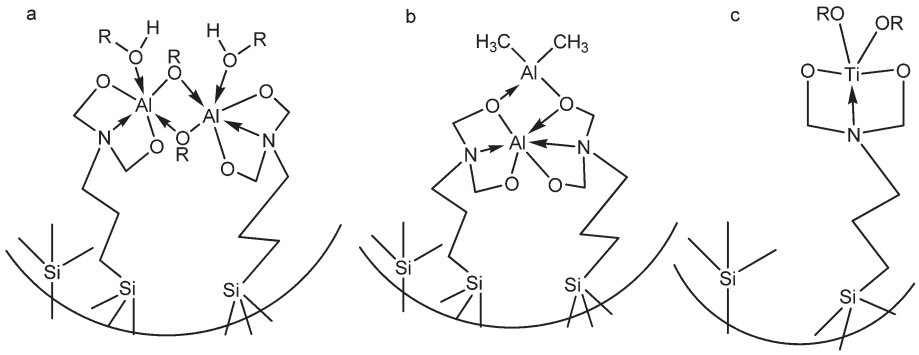

Fig. 7 Proposed structure for the different materials (a) Al-PADO-HMDS-SBA-15, (b) Al(Me)-PADO-HMDS-SBA-15 and (c) Ti-PADO-HMDS-SBA-15.

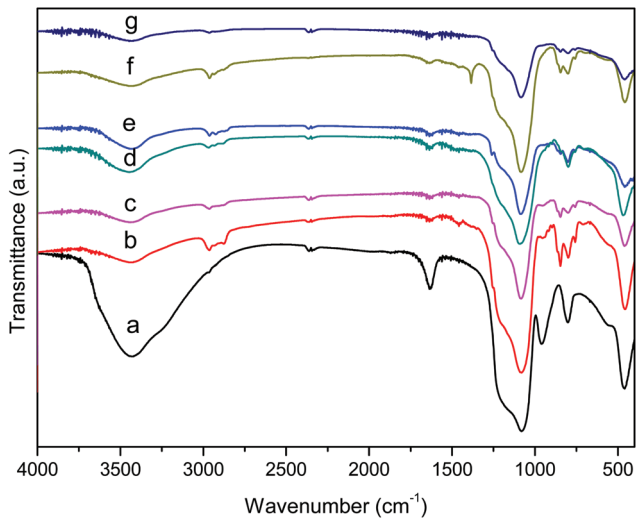

Fig. 8 FT-IR spectra of (a) SBA-15 (b) PADOH-HMDS-SBA-15 (c) Ti-PADO-HMDS-SBA-15 (d) Zn-PADO-HMDS-silica (e) Zn-PADO-HMDS-SBA-15 (f) Mg-PADO-HMDS-SBA-15 and (g) Al-PADO-HMDS-SBA-15.

bipodal and monopodal connections, the proportion of them depending on the metal content.[35] The spectra obtained for Zn and Mg-SBA-15 suggest the presence of different types of species grafted onto the silica surface, naked magnesium and zinc species, as well as butyl magnesium and methyl zinc grafted complexes.

Diffuse reflectance UV-vis spectroscopy (DRUV-vis) is a useful corroborative tool in indicating the coordination environment of titanium sites. Absorption maxima in the range of 210–240 nm are attributed to a LMCT for true four-coordinate Ti(IV). The titanium grafted sample Ti-SBA-15 spectrum (taken under ambient air conditions, Fig. 10) shows a broad absorption band in the range 210–300 nm, with a maximum at 250 nm. It has been observed that the ligand–metal charge transfer transition red shifted with increasing TiO_2 suggesting a gradual increase in the polymerization degree of titanium atoms. Based on these findings it can be deduced that the titanium atoms are mainly grafted on the wall surface of the SBA-15 by one or two O–Si–O bridges as $Ti(OSi)(OR)_3$ or $Ti(OSi)_2(OR)_2$ in partially polymerized states.[36] The DRUV-vis spectrum of Ti-PADO-HMDS-SBA-15 exhibits a

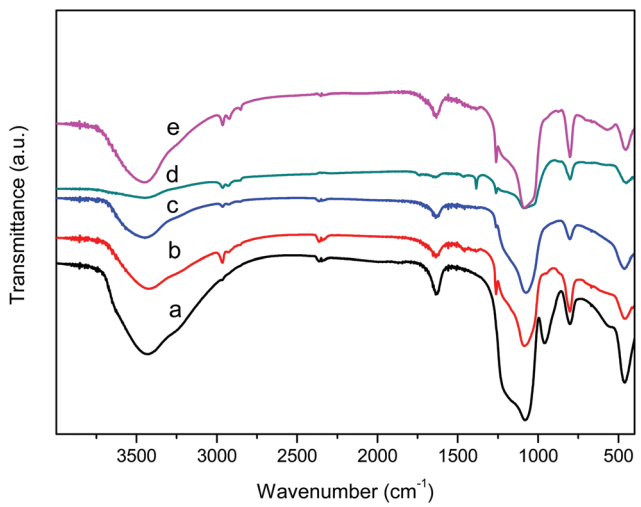

Fig. 9 FT-IR spectra of (a) SBA-15 (b) Ti-SBA-15 (c) Zn-SBA-15 (d) Mg-SBA-15 and (e) Al-SBA-15.

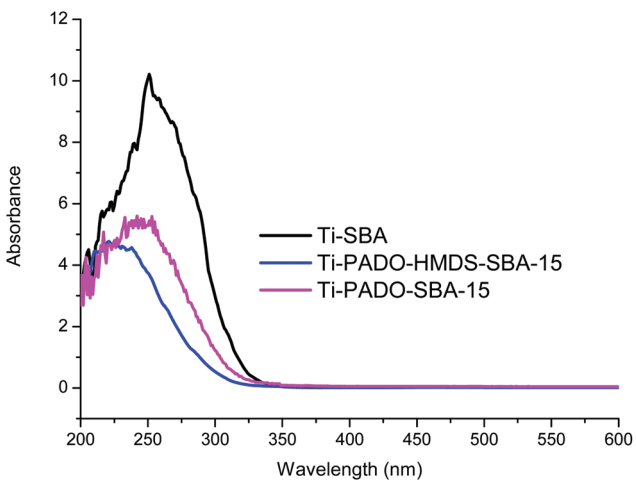

Fig. 10 DRUV-Vis spectra of Ti-SBA-15, Ti-PADO-SBA-15 and Ti-PADO-HMDS-SBA-15.

broad band in the range 240–210 nm, at λ_{max} = 210 nm for the oxygen to tetrahedral Ti(IV) charge transfer band (LMCT) and higher wavenumber values indicative of the presence of a second type of titanium species with higher coordination environments as expected due to the existence of an additional nitrogen donor atom in the ligand skeleton. For Ti-PADO-SBA-15 a shift of the broad band to a higher wavenumber value is observed (see Fig. 10). This behaviour has been observed previously by our group,[37] it seems to be that the steric crowding imposed by the trimethylsilyl groups attached to the silica surface yields spatially separated aminediol propyl units that behave as if they are isolated on the surface. However, in the absence of the protector the aminediol units attached to flexible alkyl chains may be near enough to allow some degree of oligomerization between metallic units given the higher amount of titanium in this material and the tendency of this metal to saturate its binding sphere. Therefore, it is probable that in some of the titanium complexes on the silica surface the central core consists of an inter-linked titanium isopropoxy moiety as observed frequently for these types of derivatives.[38] These results confirm that when direct reaction between silanol groups on the surface and the metal centre occurs multiple types of sites are often formed, removing the single site nature of the system. The process that immobilizes the complex *via* a covalent linkage between the ligand and the support using a multistep grafting approach seems to be a good method to obtain well defined active centres (see Fig. 7c).

ε-Caprolactone polymerization with homogeneous and supported catalysts

The ROP of ε-CL was carried out with homogeneous catalysts prepared by reaction of an EtOH solution of 3-[bis(2-hydroxyethyl)amino]propyl-triethoxysilane with $Al(O^iPr)_3$, $AlMe_3$, $Mg(^nBu)_2$, $Ti(O^iPr)_4$ or $ZnMe_2$, in dry toluene in 1 : 1 ratio. The obtained species labelled as M-PADO (M = Al, Mg, Ti and Zn) have been characterized *via* NMR and FT-IR spectroscopy (see ESI† and Fig. S5–10).

The catalytic behaviour of M-PADO systems towards ROP of ε-CL in toluene solution has been systematically examined; the results are shown in Table 3. The polymerization proceeds at room temperature in the absence of an alcohol acting as a co-initiator. The process is straightforward for titanium with 60% conversion after 24 h and more efficient for zinc and aluminium complexes in the monomer/initiator ratio 100 : 1, achieving complete conversion at room temperature in 30 min (Fig. S11†). Mg-PADO exhibits the highest activity, 100% conversion in 5 min. Nevertheless, Al-PADO provides the highest molecular weight and lowest PDI value (M_n = 22 200, PDI = 1.22). However, relatively high PDIs (1.22–1.45) of the polymers implied that side reactions such as transesterification reactions exist in the polymerization process. Fig. 11 shows the conversion *vs.* time curves of ε-caprolactone polymerization (M_0/I_0 = 300) with Al and Mg-PADO complexes. Both polymerizations proceed up to 100% conversion in a different range of time. Metal complexes required a longer time to catalyze complete polymerization when the monomer-to-catalyst ratio increases. GPC analysis reveals that the poly(ε-caprolactone) obtained shows values ranging from 9500 to 22 200. Fig. 11 also reveals some differences between the behaviour of both catalysts; unexpectedly the conversion values for Al-PADO show a linear dependence with time, suggesting that reaction is zero-order in the monomer. In addition, the kinetic studies show a linear relationship of ln(100 − C(%)) *versus* time for Mg-PADO indicating that the polymerization is first-order in the monomer, which is consistent with the living character of this polymerization. The curvature in the kinetic plot obtained for the Al-PADO system suggests a slow initiation of the process. This behaviour has previously been observed for aluminium and lanthanide alkoxy derivatives;[39,40] the existence of the aggregation process of the active species in the polymerization medium slows down the initiation step, however for higher degrees of monomer conversion the less reactive species eventually transformed almost completely into the growing species. The apparent rate constants were calculated as 10^{-4} min^{-1} for the Zn-PADO complex at (M_0/I_0) = 200

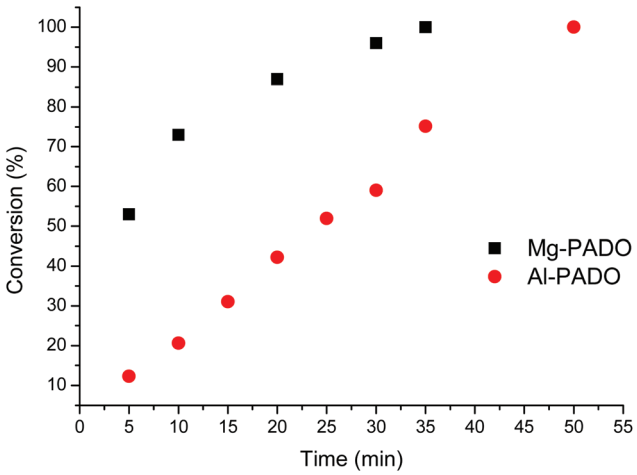

Fig. 11 Conversion *versus* reaction time for the polymerization of ε-CL ($[M_0/I_0]$ = 300, room temperature) initiated with Mg and Al-PADO complexes.

Table 3 Polymerization of ε-CL catalysed by M-PADO complexes[a]

Initiator	Monomer/initiator	Conversion[b] (%)	Time (min)	M_n	PDI[c]
Al-PADO	100 : 1	100	30	11 100	1.27
Al-PADO	200 : 1	100	50	20 600	1.29
Al-PADO	300 : 1	100	60	22 200	1.22
Mg-PADO	100 : 1	100	5	9200	1.32
Mg-PADO	200 : 1	100	30	10 700	1.33
Mg-PADO	300 : 1	100	35	11 100	1.33
Ti-PADO	100 : 1	60	1440	15 200	1.42
Zn-PADO	100 : 1	100	30	9500	1.32
Zn-PADO	200 : 1	100	1440	—	—

[a] Reaction conditions: 100 mg of the homogeneous catalyst, room temperature, toluene as the solvent. [b] Determined by ^{1}H NMR analysis. [c] Measured by GPC at 27 °C in THF relative to polystyrene standards.

(Fig. S12†), and 0.118 min^{-1} for Mg-PADO complexes at (M_0/I_0) = 300 (Fig. S13†).

Previous studies with titanium and aluminium alkoxy complexes showed that the ring opening polymerization of ε-caprolactone proceeds *via* a coordination–insertion reaction through the formation of a coordination complex between the lactone and the initiator with interactions between the carbonyl group and the metal atom. Then, the ring opening reaction occurs with a selective cleavage of the acyl–oxygen bond. To corroborate such a mechanism in the titanium and aluminium case, the identification of end groups of the synthesized polymer isolated at a low conversion rate to enhance the end group concentration was carried out. We confirmed by ^{1}H NMR spectroscopy the presence of signals corresponding to the –CH_2–OH end group at 3.63 ppm in both spectra. In the titanium case a signal attributed to the methyl groups of isopropyl ester function (–COOCH(CH_3)$_2$) at 4.90 ppm is present indicating that the growing end groups are isopropoxy groups bonded to titanium (Fig. S14†). In the aluminium case, EtOH present in the reaction media during the synthesis of the complex acts as an initiator and the ethoxy group directly bonded to the metal centre; the mechanism end-group analysis supports this proposal since in the ^{1}H NMR spectrum of isolated ε-PCL a triplet due to the methyl and methylene groups of the ethyl ester function as a growing end group appears at 1.21 and 4.08 ppm, respectively (Fig. S15†). The ROP polymerization process using the magnesium complex as the catalyst seems to proceed in a similar way; the presence of EtOH during the synthesis procedure guarantees its coordination to the magnesium centre; the growing end group is an ethyl ester function which is confirmed from the ^{1}H NMR spectrum of the isolated polymer (Fig. S16†).

Fig. 12 shows the ^{1}H NMR spectrum of a PCL polymer obtained by using Zn-PADO as the initiator by taking an aliquot of the toluene solution without hydrolysis. Besides signals due to the protons along the polymer backbone, signals due to the polymer's end groups can also be observed. The signals at 1.17–1.24, 2.57 and 2.73 ppm indicate that the PCL is probably attached with a –OCH_2N–CH_2–CH_2– group, which suggests, in principle, the behaviour of the ancillary ligand as the alkoxy growing group and ROP may not be regarded as a living one.

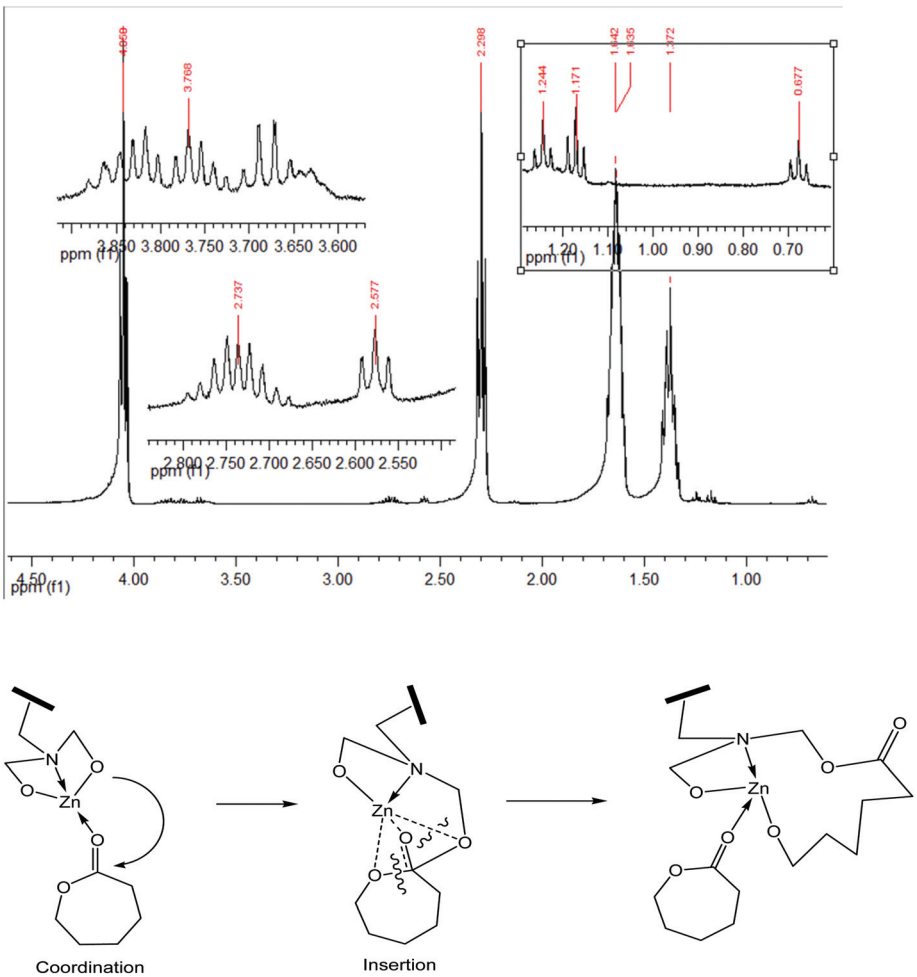

Fig. 12 ^{1}H NMR spectrum (measured in $CDCl_3$, 400 MHz) of the polymer isolated from the polymerization of ε-CL initiated with Zn-PADO (M_0/I_0 = 100, at r.t.). The proposed coordination insertion mechanism.

Table 4 Polymerization of ε-CL in the presence of supported catalysts[a]

Initiator/co-initiator	Conversion[b] (%)	M_n	PDI[c]
Al-SBA-15	100	37 900	1.44
Mg-SBA-15/BnOH	12	—	—
Ti-SBA-15	100	6900	1.20
Zn-SBA-15	47	5000	1.09
Al-PADO-HMDS-SBA-15	11	—	—
Mg-PADO-HMDS-SBA-15/BnOH	100	<3000	—
Ti-PADO-HMDS-SBA-15	10	—	—
Zn-PADO-HMDS-SBA-15	60	5100	1.11
Zn-PADO-HMDS-Silica	35	4200	1.19

[a] Reaction conditions: 100 mg of the heterogeneous catalyst, $[M_0/I_0]$ = 100, temperature = 80 °C, toluene as the solvent, reaction time 24 h. [b] Determined by ^{1}H NMR spectroscopy analysis. [c] Measured by GPC at 27 °C in THF relative to polystyrene standards.

The results of ε-CL polymerization with heterogeneous catalysts are summarized in Table 4. As can be seen the active heterogeneous Ti-SBA-15, Zn-SBA-15 and Zn-PADO-HMDS-SBA-15 catalysts formed poly(ε-caprolactone) with lower PDI values than those achieved with the homogeneous catalysts. In addition, for the M-SBA-15 (M = Ti, Zn, Al, Mg) supported catalyst, those materials prepared by direct reaction of an alkoxy complex, $M(OR)_n$, (M = Ti, Al) show better conversion values with respect to those prepared using alkyl complexes, MR_n (M = Zn, Mg) as metallic precursors. In fact, using Ti-SBA-15 or Al-SBA-15 as the initiator 100% conversion is reached in 24 hours and the molecular weight of PLA produced with Al-SBA-15 is approximately 5.5 times higher than the PCL made with Ti-SBA-15 or Zn-SBA-15. The Mg-SBA-15 material is inactive for the polymerization under the experimental conditions studied, benzyl alcohol was used as a co-initiator, but even in the presence of benzyl alcohol the conversion values are very low (only 12%). This is probably due to that initiation is faster in the presence of the metal–O^{i}Pr bond in Ti and Al-SBA-15 as demonstrated by using ^{1}H NMR to study the synthesized polymer (Fig. S17 and S18†). After appropriate work up with isopropanol and isolation the recovered polymers show a very narrow molecular weight distribution and a symmetrical monomodal elution peak is observed, which indicates the complete absence of residual silica in the recovered polymer (see Fig. S19†).[22]

The initiation mechanism can be unambiguously established as a coordination–insertion mechanism *via* an acyl–oxygen bond cleavage due to identification of isopropoxy –O–$CH(CH_3)_3$ and hydroxyl –CH_2–OH end groups of the synthesized polymer. In the system Zn–SBA-15 initiation could be assumed to occur *via* a Zn–OSi bond.[41] Alternatively, the study by ^{1}H NMR spectroscopy of the so obtained polymer shows a triplet at 3.62 ppm assigned to the hydroxyl end group, –CH_2–OH, and a singlet signal at 3.64 ppm which can be assigned to a methoxy group –OCH_3 on the other end (Fig. 13). Since the presence of methyl groups bonded to the grafted zinc atoms is supported by the infrared studies, a nucleophilic attack onto the monomer by the methyl group cannot be discarded.[42]

A kinetic study was carried out using the Ti-SBA-15 material (Fig. S20†). The conversion value increases gradually with time, which suggests the accessibility of the titanium centres and the absence of mass transfer limitations. In addition, the kinetic studies show a linear relationship of ln(100 − C(%)) *versus* time (Fig. S21†). The linearity obtained indicated that the polymerization is first-order in the monomer, which is consistent with the living character of this polymerization.

In comparison the tethered systems show better conversion values in the case of Zn-PADO-HMDS-SBA-15 (with a conversion of 60% after 24 h) and Mg-PADO-HMDS-SBA-15 (with a conversion of 100% after 24 h), the latter in the presence of benzyl alcohol as the co-initiator. In contrast, Ti and

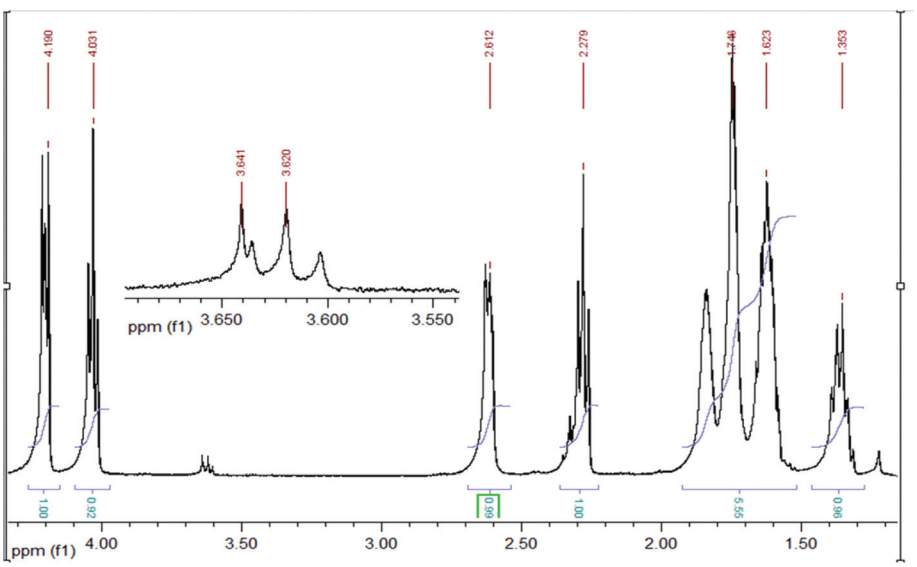

Fig. 13 ^{1}H NMR spectrum (measured in $CDCl_3$, 400 MHz) of the polymer isolated from the polymerization of ε-CL initiated with Zn-SBA-15 (M_0/I_0 = 100, at r.t.).

Al-PADO-HMDS-SBA-15 are shown to be very poor catalysts. Molecular weights of polymers produced by the most active zinc and aluminium heterogeneous systems decrease in comparison with their homogeneous counterparts. A remarkable fact is that the Zn-PADO-HMDS-SBA-15 catalyst exhibited a higher polymerization activity (TOF = 2.5 h^{-1}) than the Zn-PADO-HMDS-silica catalyst (TOF = 1.5 h^{-1}). In addition, the PCL obtained by using the Zn-PADO-HMDS-SBA-15 catalyst presents a higher molecular weight and slightly lower polydispersity index than that achieved with Zn-PADO-HMDS-silica. These results suggest that the properties of the support may play an important role in the polymerization reaction.

The end group analysis of the polymer obtained using Zn-PADO-HMDS-SBA-15 as the initiator was conducted (Fig. S22†). Since the only significant signal observed in the ^{1}H NMR spectrum is the triplet assigned to the hydroxyl end group, a similar mechanism to those observed for the homogeneous system is proposed, *i.e.* the nucleophilic attack on the monomer by the ancillary chelated ligand. Finally, the mechanism for the polymerization process using Mg-PADO-HMDS-SBA-15 as the catalyst and benzyl alcohol as the co-initiator has been studied in a similar way (Fig. S23†). In this case in the ^{1}H NMR spectra a singlet signal appears at 5.05 ppm attributed to the methylene group of the –O–CH_2–Ph capped benzyl alcoxy group, demonstrating the existence of a coordination–insertion mechanism as well.

The polymers produced with the most active catalysts have been studied by scanning electron microscopy. The morphologies of PCL produced from Ti-SBA-15 (Fig. 14b) and Zn-PADO-HMDS-SBA-15 (Fig. 14c) are irregular demonstrating that there is no replication phenomenon, common in the heterogeneous polymerization of olefins. As can be seen from Fig. 14a the particle is clearly an assembly of smaller structures, which supports the presence of active sites on the silica surface; monomer diffused through the pores of SBA-15 adsorbs on the layer of the polymer surrounding the catalyst and diffuses through this layer to the active sites on the surface where polymerization takes place.[43] In comparison,

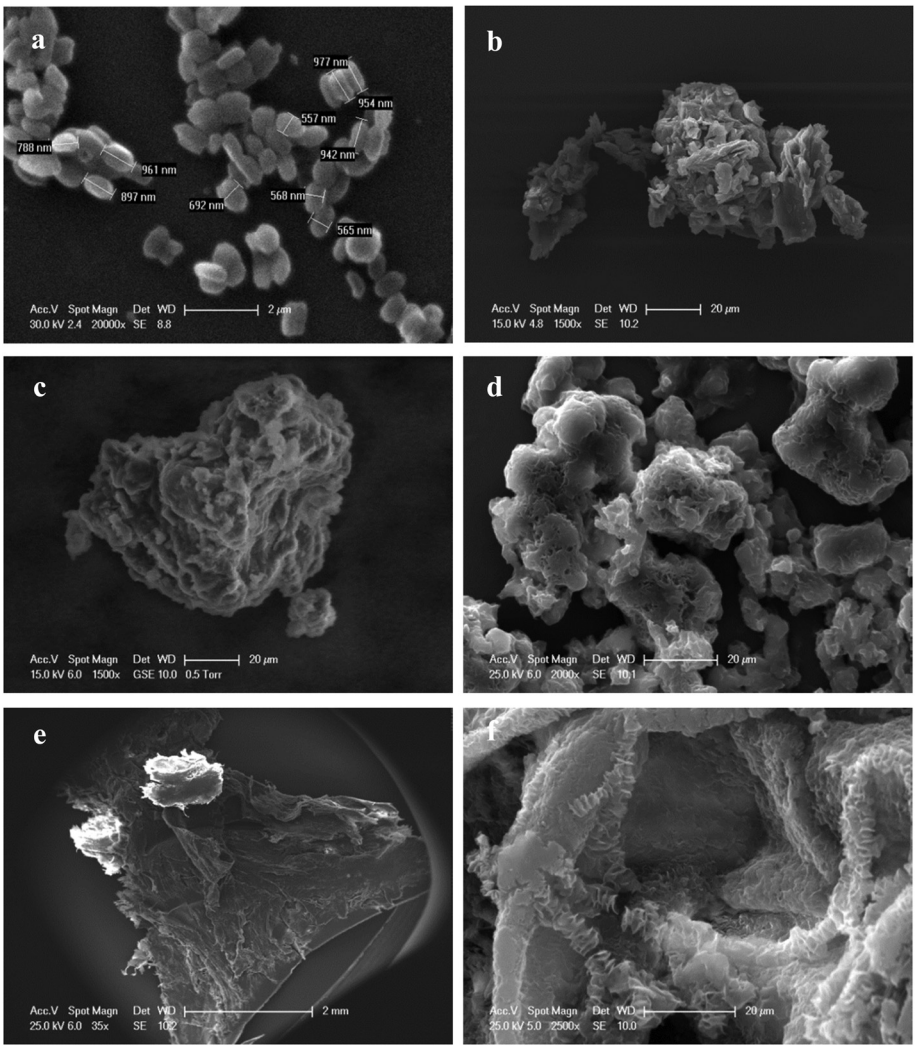

Fig. 14 SEM micrographs of (a) SBA-15 (b) PLC produced from Ti-SBA-15 (c) PLC produced from Zn-PADO-HMDS-SBA-15 (d) PLC produced from Zn-PADO (e) and (f) PLC produced from Al-SBA-15.

the morphology of the polymer obtained from the homogeneous complex Zn-PADO (Fig. 14d) is also irregular, supporting the existence of comparable active single sites on the silica surface when using Zn-PADO-HMDS-SBA-15 (Fig. 14c).

The morphology of the more flexible polymer obtained by using Al-SBA-15 (Fig. 14e and f) as the catalyst is very different as expected taking into account the higher molecular weight of this material. Irregular folded layers are observed.

A recycling experiment has been performed with Ti-SBA-15 by adding isopropanol to the polymerization medium when the monomer conversion is complete. The addition of an alcohol has two roles: release of the polymer and regeneration of the isopropoxy groups bonded to titanium on the silica surface. In the first step PCL was initiated by using Ti-SBA-15 in toluene at 80 °C, after 24 h monomer conversion, isopropanol was added to the living polyester chains in order to separate them from the support and the solid catalyst was allowed to settle. The supernatant polymer solution was separated by filtration and the catalyst was washed with dichloromethane and dried under vacuum. The ε-CL polymerization was repeated under similar experimental conditions by using the recovered Ti-SBA-15 and it was possible to achieve 72% conversion, which confirms the reusability of the catalyst. The stability of the reused Ti-SBA-15-R catalyst was examined by FT-IR analysis. The FT-IR spectrum of the Ti-SBA-15-R catalyst shows bands characteristic of SBA-15 and those corresponding to isopropoxy groups bonded to titanium. In addition the band observed at 1724 cm^{-1} is attributed to the presence of some amount of the polymer (Fig. 15). Thermogravimetric analysis of the recovered Ti-SBA-15-R catalyst (Fig. 16) shows a weight loss in the range 185–350 °C attributed to the degradation of isopropoxy ligands bonded to the titanium centre supporting the catalyst regeneration. The TG curve does not show thermal degradation between 376 °C and 480 °C which would correspond to PCL decomposition.[44] In addition, these experiments suggest, firstly, that the decrease in the activity may be due to the small amount of the polymer bonded to titanium and secondly that the removal of metal residues in the polymer chain is possible by adding an alcohol after polymerization. Therefore, a pure metal-free polymer product can be obtained.

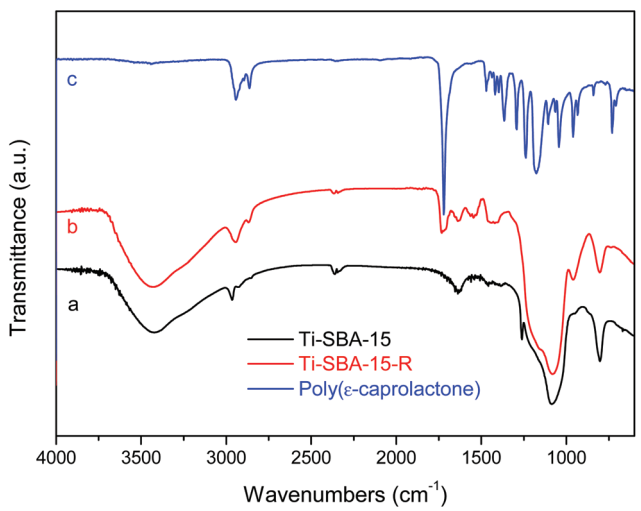

Fig. 15 FT-IR spectra of (a) Ti-SBA-15, (b) Ti-SBA-15-R and (c) poly-(ε-caprolactone).

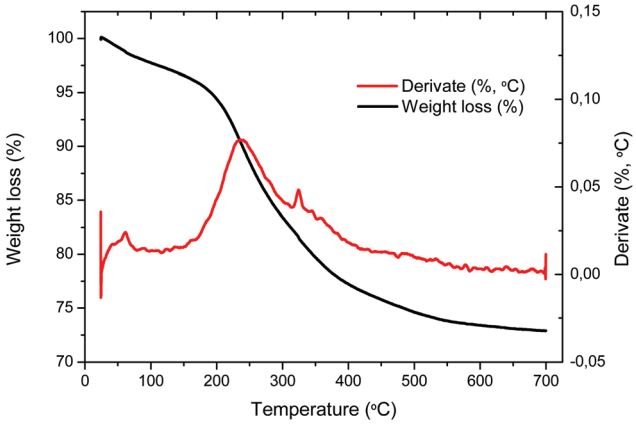

Fig. 16 Thermogravimetric analysis of Ti-SBA-15-R.

Conclusions

In a toluene solution heterogeneous and homogeneous systems have demonstrated to be active initiators for the ROP of ε-CL. The heterogeneous catalysts required significantly longer reaction times than their homogeneous counterparts; this is presumably due to mass transport effects in the solid-supported materials. The heterogeneous Ti-SBA-15, Zn-SBA-15 and Zn-PADO-HMDS-SBA-15 catalysts produced poly(ε-caprolactone) with a narrow molecular weight distribution, close to one. The support plays an important role, as can be concluded by comparing Zn-PADO-HMDS-SBA-15 and Zn-PADO-HMDS-silica systems, the former showing higher activity values and producing polymers with higher molecular weight and narrower polydispersity. In addition, the recovery experiments carried out for the Ti-SBA-15 system show the reusability of heterogeneous catalysts.

Acknowledgements

We gratefully acknowledge financial support from the Ministerio de Educación y Ciencia, Spain (project CTQ2012-30762).

References

1 Green paper packaging and sustainability: an open dialogue between stakeholders. European, 2011. http://www.europen.be/index.php?action=onderdeel&onderdeel=5&titel=News+Room&categorie= 1&item=121.

2 S. Martinez-Diaz, N. Garcia-Giralt, M. Lebourg, J.-A. Gómez-Tejedor, G. Vila, E. Caceres, P. Benito, M. Monleón Pradas,

X. Nogues, J. L. Gómez Ribelles and J. Carles Monllau, *Am. J. Sports Med.*, 2010, **38**, 3509.
3 H. Seyednejad, A. H. Ghassemi, C. F. van Nostrum, T. Vermonden and W. E. Hennink, *J. Controlled Release*, 2011, **152**, 168.
4 Y. Oda, H. Asari, T. Urakami and K. Tonomura, *J. Ferment. Bioeng.*, 1995, **80**, 265.
5 L. S. Naira and C. T. Laurencin, *Prog. Polym. Sci.*, 2007, **32**, 762.
6 I. Vroman and L. Tighzert, *Materials*, 2009, **2**, 307.
7 K. M. Stridsberg, M. Ryner and A.-C. Albertsson, *Adv. Polym. Sci.*, 2002, **157**, 42.
8 J. Cayuela, V. Bounor-Legaré, P. Cassagnau and A. Michel, *Macromolecules*, 2006, **39**, 1338.
9 D. J. Darensbourg, P. Ganguly and D. Billodeaux, *Macromolecules*, 2005, **38**, 5406.
10 T. M. Ovitt and G. W. Coates, *J. Am. Chem. Soc.*, 2002, **124**, 1316.
11 D. J. Darensbourg and O. Karroonnirun, *Organometallics*, 2010, **29**, 5627.
12 L. R. Rieth, D. R. Moore, E. B. Lobkovsky and G. W. Coates, *J. Am. Chem. Soc.*, 2002, **124**, 15239.
13 L. Wang and H. Ma, *Macromolecules*, 2010, **43**, 6535.
14 B. J. O'Keefe, L. E. Breyfogle, M. A. Hillmyer and W. B. Tolman, *J. Am. Chem. Soc.*, 2002, **124**, 4385.
15 A. Otero, A. Lara-Sanchez, J. Fernandez-Baeza, C. Alonso-Moreno, I. Marquez-Segovia, L. F. Sanchez-Barba, J. A. Castro-Osma and A. M. Rodríguez, *Dalton Trans.*, 2011, **40**, 4687.
16 C.-Y. Li, C.-J. Yu and B.-T. Ko, *Organometallics*, 2013, **32**, 172.
17 A. K. Sutar, T. Maharana, S. Dutta, C. T. Chen and C. C. Lin, *Chem. Soc. Rev.*, 2010, **39**, 1724.
18 J. Wu, T.-L. Yu, C.-T. Chen and C.-C. Lin, *Coord. Chem. Rev.*, 2006, **250**, 602.
19 A. Arbaoui and C. Redshaw, *Polym. Chem.*, 2010, **1**, 801.
20 E. Kim, E. W. Shin, I.-K. Yoo and J. S. Chung, *J. Mol. Catal. A: Chem.*, 2009, **298**, 36.
21 J. H. Khan, F. Schue and G. A. George, *Polym. Int.*, 2010, **59**, 1506.
22 E. Martin, P. Dubois and R. Jérôme, *Macromolecules*, 2003, **36**, 7094.
23 K. Tortosa, T. Hamaide, C. Boisson and R. Spitz, *Macromol. Chem. Phys.*, 2001, **202**, 1156.
24 K. Yu and C. W. Jones, *J. Catal.*, 2004, **222**, 558.
25 C. D. Iulio, M. D. Jones, M. F. Mahon and D. C. Apperley, *Inorg. Chem.*, 2010, **49**, 10232.
26 C. D. Iulio, M. D. Jones and M. F. Mahon, *J. Organomet. Chem.*, 2012, **718**, 96.
27 W. Long, C. S. Gill, S. Choi and C. W. Jones, *Dalton Trans.*, 2010, **39**, 1470.
28 N. Wanna, T. Kraithong, T. Khamnaen, P. Phiriyawirut, S. Charoenchaidet and J. Tantirungrotechai, *Catal. Commun.*, 2014, **45**, 118.
29 (*a*) D. Zhao, Q. Huo, J. Feng, B. F. Chmelka and G. D. Stucky, *J. Am. Chem. Soc.*, 1998, **120**, 6024; (*b*) M. Choi, W. Heo, F. Kleitz and R. Ryoo, *Chem. Commun.*, 2003, 1340.
30 I. Hierro, Y. Pérez and M. Fajardo, *J. Solid State Electrochem.*, DOI: 10.1007/s10008-014-2496-x.
31 P. Zarabadi-Poor, A. Badiei, B. D. Fahlman, P. Arab and G. Mohammadi Ziarani, *Ind. Eng. Chem. Res.*, 2011, **50**, 10036.
32 R. Ballesteros, Y. Pérez, M. Fajardo, I. Sierra and I. Hierro, *Microporous Mesoporous Mater.*, 2008, **116**, 460.
33 P. Soubayrol, G. Dana and P. P. Man, *Magn. Reson. Chem.*, 1996, **34**, 638.
34 E. Pretsch, T. Clero, J. Seibl and W. Simon, *Tablas para la elucidación estructura de compuestos orgánicos por métodos espectroscópicos*, ed. J. Castells and F. Camps, Alhambra, 1980.
35 P. Iengo, G. Aprile, M. D. Serio, D. Gazzoli and E. Santacesari, *Appl. Catal., A*, 1999, **178**, 97.
36 J. E. Haskouri, S. Cabrera, M. Gutierrez, A. Beltrán-Porter, D. Beltrán-Porter, M. D. Marcos and P. Amorós, *Chem. Commun.*, 2001, 309.
37 P. G. Lampman and G. Kriz, *Introduction to spectroscopy*, Harcourt College Publishers, USA, 2001.
38 A. O. Bouth, G. L. Rice and S. L. Scott, *J. Am. Chem. Soc.*, 1999, **121**, 7201.
39 B. M. Chamberlain, B. A. Jazdzewski, M. Pink, M. A. Hillmyer and W. B. Tolman, *Macromolecules*, 2000, **33**, 3970.
40 A. Kowalski, A. Duda and S. Penczek, *Macromolecules*, 1998, **31**, 2114.
41 M. D. Jones, M. G. Davidson, C. G. Keir, A. J. Wooles, M. F. Mahon and D. C. Apperley, *Dalton Trans.*, 2008, 3655.
42 M. Vivas and J. Contreras, *Eur. Polym. J.*, 2003, **39**, 43.
43 T. F. McKenna and J. B. P. Soares, *Chem. Eng. Sci.*, 2001, **56**, 3931.
44 A. Mohamed, V. L. Finkenstadt, S. H. Gordon, G. Biresaw, E. Palmquist Debra and P. Rayas-Duarte, *J. Appl. Polym. Sci.*, 2008, **110**, 3256.